





# Somatic MAP3K3 and PIK3CA mutations in sporadic cerebral and spinal cord cavernous malformations

Tao Hong,<sup>1,†</sup> Xiao Xiao,<sup>2,†</sup> Jian Ren,<sup>1,†</sup> Bing Cui,<sup>2</sup> Yuru Zong,<sup>2</sup> Jian Zou,<sup>3</sup> Zqi Kou,<sup>3</sup> Nan Jiang,<sup>1</sup> Guolu Meng,<sup>1</sup>  Gao Zeng,<sup>1</sup> Yongzhi Shan,<sup>1</sup> Hao Wu,<sup>1</sup> Zan Chen,<sup>1</sup> Jiantao Liang,<sup>1</sup> Xinru Xiao,<sup>1</sup> Jie Tang,<sup>1</sup> Yukui Wei,<sup>1</sup> Ming Ye,<sup>1</sup> Liyong Sun,<sup>1</sup> Guilin Li,<sup>1</sup> Peng Hu,<sup>1</sup> Rutai Hui,<sup>2</sup> Hongqi Zhang<sup>1</sup> and  Yibo Wang<sup>2</sup>

<sup>†</sup>These authors contributed equally to this work.

Cavernous malformations affecting the CNS occur in ~0.16–0.4% of the general population. The majority (85%) of cavernous malformations are in a sporadic form, but the genetic background of sporadic cavernous malformations remains enigmatic. Of the 81 patients, 73 (90.1%) patients were detected carrying somatic missense variants in two genes: MAP3K3 and PIK3CA by whole-exome sequencing. The mutation spectrum correlated with lesion size ( $P = 0.001$ ), anatomical distribution ( $P < 0.001$ ), MRI appearance ( $P = 0.004$ ) and haemorrhage events ( $P = 0.006$ ). PIK3CA mutation was a significant predictor of overt haemorrhage events ( $P = 0.003$ , odds ratio = 11.252, 95% confidence interval = 2.275–55.648). Enrichment of endothelial cell population was associated with a higher fractional abundance of the somatic mutations. Overexpression of the MAP3K3 mutation perturbed angiogenesis of endothelial cell models *in vitro* and zebrafish embryos *in vivo*. Distinct transcriptional signatures between different genetic subgroups of sporadic cavernous malformations were identified by single cell RNA sequencing and verified by pathological staining. Significant apoptosis in MAP3K3 mutation carriers and overexpression of GDF15 and SERPINA5 in PIK3CA mutation carriers contributed to their phenotype. We identified activating MAP3K3 and PIK3CA somatic mutations in the majority (90.1%) of sporadic cavernous malformations and PIK3CA mutations could confer a higher risk for overt haemorrhage. Our data provide insights into genomic landscapes, propose a mechanistic explanation and underscore the possibility of a molecular classification for sporadic cavernous malformations.

- 1 Department of Neurosurgery, Xuanwu Hospital, Capital Medical University, China International Neuroscience Institute, Beijing, China
- 2 State Key Laboratory of Cardiovascular Disease, Fuwai Hospital, National Center for Cardiovascular Diseases, Chinese Academy of Medical Sciences and Peking Union Medical College, Beijing, China
- 3 The Institute of Translational Medicine, Zhejiang University, Hangzhou 310058, China

Correspondence to: Yibo Wang, PhD  
Fuwai Hospital, Chinese Academy of Medical Sciences and Peking Union Medical College  
167 Beilishi Rd, Beijing 100037, China  
E-mail: yibowang@hotmail.com

Received December 24, 2020. Revised March 01, 2021. Accepted March 07, 2021. Advance access publication March 17, 2021

© The Author(s) (2021). Published by Oxford University Press on behalf of the Guarantors of Brain. All rights reserved.

For permissions, please email: journals.permissions@oup.com

Correspondence may also be addressed to: Hongqi Zhang, MD, PhD  
Department of Neurosurgery, Xuanwu Hospital  
Capital Medical University, 45 Changchun St, Beijing, 100053, China  
E-mail: xwzhanghq@163.com

**Keywords:** MAP3K3; PIK3CA; somatic mutation; cavernous malformations; haemorrhage

**Abbreviations:** CM = cavernous malformation; ddPCR = droplet digital polymerase chain reaction; WES = whole-exome sequencing

## Introduction

Cavernous malformations (CMs) are among the most prevalent vascular malformations affecting the CNS and occur in ~0.16–0.4% of the general population.<sup>1–3</sup> CMs can present incidentally, with seizures or focal neurological deficits most frequently due to haemorrhages.<sup>4</sup> Neurosurgical resection remains the only effective treatment, which is limited by lesion accessibility and is associated with non-negligible rates of morbidity and mortality.<sup>5,6</sup> CMs tend to fall into two categories: familial (inherited) forms and sporadic forms, with the majority (85%) being sporadic.<sup>7,8</sup> The genetic analysis of CMs was mostly based on the inherited form of CMs and was associated with three distinct loci: CCM1 (*KRIT1*), CCM2 and CCM3 (*PDCD10*).<sup>9–11</sup> Heterozygous loss-of-function of these three mutations was identified in ~90% of familial cases.<sup>5</sup> Previous genetic studies on sporadic CMs mainly focused on the known three CCM genes using PCR amplicons, while the detection rate of pathogenic mutations was low.<sup>12–14</sup> The genetic background of sporadic CMs remains unclear. Recently, pathogenic somatic mutations have been identified in sporadic arteriovenous malformations, capillary malformations, lymphatic malformations and some types of venous malformations.<sup>15–19</sup> We hypothesized that sporadic CMs also arise from somatic mutations in the vasculature of the CNS.

## Materials and methods

### Study populations

We used whole-exome sequencing (WES) to detect potential pathogenic somatic mutations within the CM lesions and evaluate the possibility of correlating molecular subgroups with clinical characteristics. Patients were eligible for inclusion if they had cerebral or spinal cord CMs with negative family history. The diagnosis of CM was based on the typical appearance of the lesion on MRI and pathological examination of resected samples. Catheter angiography was not used in the evaluation of CMs, unless a differential diagnosis of arteriovenous malformation is being considered. Ninety patients with CMs in the CNS who underwent surgical resection of the lesions at the Beijing Xuanwu Hospital in China between May 2017 and November 2019 were recruited to this study. The study was approved by the ethics committee of Beijing Xuanwu Hospital (no. 2016032) and written informed consent from all patients or their guardians was obtained before surgery.

### Clinical characteristics

All medical information was extracted from a computerized online database, which contained demographics, clinical, radiological, and treatment-related information. We defined a haemorrhage event as a symptomatic event with radiographic evidence of overt haemorrhage.<sup>6</sup> The observational period of haemorrhage was defined as the interval between the initial diagnosis and surgical treatment. The MRI appearance of CMs were classified into three types based on the Zabramski classification.<sup>15</sup> Type I was defined

as lesions with high signal intensity cores on T<sub>1</sub>-weighted imaging and high/low signal intensity on T<sub>2</sub>-weighted imaging. Type II was defined as lesions with reticulated, mixed-signal intensity cores on T<sub>1</sub>- and T<sub>2</sub>-weighted imaging (with surrounding dark rim). Type III was defined as lesions with iso-to-low signal intensity on T<sub>1</sub>-weighted imaging and low signal intensity on T<sub>2</sub>-weighted imaging. All films were reviewed by independent neuroradiologists. The Karnofsky Performance Scale score was used to provide an objective measure defining neurological functional status of the patients with cerebral or spinal cord CMs. The neurological status of patients with spinal cord CMs were further assessed by the modified McCormick scale.<sup>16</sup>

### Genetic analysis and functional studies

We performed WES on fresh-frozen tissue samples of CMs. Sequencing depth was anticipated to be 200–300× for tissue samples. We confirmed the results with droplet digital PCR (ddPCR) analysis to observe mitogen-activated protein kinase kinase 3 (*MAP3K3*) mutation and phosphatidylinositol-4,5-bisphosphate 3-kinase catalytic subunit  $\alpha$  (*PIK3CA*) mutations. We also compared variant frequencies of the somatic mutations in endothelial cells and non-endothelial cells of tissue samples using fluorescence-activated cell sorting (FACS) and ddPCR. The functional studies of *PIK3CA* on endothelial cells and animal models have been well performed in previous studies on venous malformations.<sup>17,18</sup> We explored the functions of the *MAP3K3* (p.Ile441Met) mutation in human umbilical vein endothelial cells (HUVECs) and in a zebrafish model.

### Single cell transcriptome analysis

Single cell RNA sequencing analyses (10× Genomics) were performed in six samples of sporadic CMs with somatic mutations of *MAP3K3* and/or *PIK3CA* and three control samples. Protein expression was assessed with immunofluorescence staining of tissues.

### Statistical analysis

We used Fisher's exact test or Pearson's  $\chi^2$  test for categorical variables and Student's t-test for continuous variables. Logistic regression analysis was used to assess the impact of multiple variables that predicted an overt haemorrhage event. Cumulative rates of haemorrhage during follow-up were illustrated using the Kaplan-Meier method, and the curves were compared by the log-rank test. All analyses were performed under the guidance of a statistician using SPSS software (version 25, IBM Corp., Armonk, New York, USA). All *P*-values are two-sided, and we defined statistical significance as *P* < 0.05.

### Data availability

The authors confirm that the data supporting the findings of this study are available within the article and its [Supplementary](#)

**material.** Derived data supporting the findings of this study are available from the corresponding author on request.

## Results

### Baseline characteristics of the patients

Ninety consecutive patients were included in the study. WES was performed in 90 fresh-frozen tissue samples of cerebral or spinal cord CMs and two associated cutaneous CMs (Patients 45 and 75). Among these, nine patients were excluded because of carrying germline non-synonymous mutations of *KRIT1* (5/9), *CCM2* (3/9) and *PDCD10* (1/9) by WES. Samples from 81 sporadic patients were eligible for final analysis, including 36 cerebral CMs and 45 spinal cord CMs. Among the 81 patients, 43 (53.1%) were male. The mean age on admission was  $37.9 \pm 15.7$  years (ranging from 3 to 82 years). The clinical characteristics of the patients are summarized in [Supplementary Table 1](#) and [Supplementary Fig. 1](#).

### Observation of MAP3K3 and PIK3CA somatic variants in patients

Of the 81 sporadic patients, WES and ddPCR resulted in the identification of somatic missense variants in *MAP3K3* and *PIK3CA* in 73 (90.1%) patients ([Fig. 1](#) and [Supplementary Fig. 2](#)). The finding of ddPCR was consistent with the results of WES ( $r = 0.882$ ,  $P < 0.001$ ). Among the 73 patients, 42 (57.5%) were detected as having an *MAP3K3* missense variant (RefSeq accession number NM\_002401.3, c.1323C>G, p.Ile441Met) with variant frequencies ranging from 0.4% to 22.7%. The same somatic mutation has been identified in verrucous venous malformations with mutant allele frequencies ranging from 6% to 19% in affected tissue.<sup>19</sup> WES of the associated cutaneous CMs in two patients with spinal cord CMs demonstrated the same *MAP3K3* mutations (p.Ile441Met) as the spinal cord CMs. *PIK3CA* hotspot activating mutations were detected in 45 (61.6%) of the 73 patients, with variant frequencies ranging from 0.4% to 24.4%. *PIK3CA* (NM\_006218.2) mutations were found in exon 7: c.1258T>C (p.Cys420Arg), in exon 9: c.1624G>A (p.Glu542Lys), c.1633G>A (p.Glu545Lys); and in exon 20: c.3140A>G (p.His1047Arg). Herein, 14 (19.2%) of the 73 sporadic patients had co-occurred somatic mutations in *MAP3K3* and *PIK3CA*. Genomic coordinates and reference genome of each mutation are described in [Supplementary Table 2](#). For simplicity, we used p.I441M, p.C420R, p.E542K, p.E545K and p.H1047R in this manuscript when referring to these mutations, respectively. Of the samples from the 81 patients with sporadic CMs, we did not find any somatic non-synonymous mutations of the three CCM genes (*KRIT1*, *CCM2* and *PDCD10*).

### The somatic mutation genotype was associated with clinical phenotype, especially in haemorrhage

We compared the clinical characteristics of the 73 patients with somatic mutations of *MAP3K3* and/or *PIK3CA* ([Tables 1](#) and [2](#)). Notably, we found that mutational profiles were correlated with risk of haemorrhage events ( $P = 0.006$ ; [Table 1](#) and [Fig. 2A](#)). Regarding overt haemorrhage events, a univariate analysis revealed that *PIK3CA* mutations were associated with a statistically significant increase in the likelihood of overt haemorrhage events [ $P = 0.002$ , odds ratio (OR) = 6.182, 95% confidence interval (CI) = 1.913–19.974; [Table 2](#)]. In the multivariate analysis, *PIK3CA* mutations were still a significant predictor of overt haemorrhage events ( $P = 0.003$ , OR = 11.252, 95% CI = 2.275–55.648; [Table 2](#)). Using the log-rank test for haemorrhage-free survival, we noted statistically significantly higher incidence of haemorrhagic events during

follow-up in lesions with *PIK3CA* mutations than those with *MAP3K3* mutations ( $P = 0.012$ ; [Fig. 2B](#)). The haemorrhagic risk during the follow-up period of the double mutation group was in-between, as expected; however, the  $P$ -value for the difference between the three genotypes did not achieve statistical significance, though a trend was observed ( $P = 0.051$ ; [Fig. 2B](#)).

The mutations spectrum was also correlated with anatomical distribution ( $P < 0.001$ ), size of lesions ( $P = 0.001$ ), and the MRI appearance ( $P = 0.004$ ). The *MAP3K3* mutation was predominantly identified in 80.5% of spinal cord CMs and 31.2% of cerebral CMs. The size of lesions carrying *PIK3CA* mutations was significantly larger ( $P = 0.001$ ; [Table 1](#)) than the other two genotypes. The majority (60.0%) of patients with *PIK3CA* mutations had a Zabramski type I appearance of MRIs. While in patients with *MAP3K3* mutations, only 28.6% had a Zabramski type I appearance. In patients with co-occurred mutations, Zabramski type II (53.3%) was the dominant MRI appearance.

### The somatic mutations mainly occurred in CD31+ cells

To identify the types of cells that have *MAP3K3* or *PIK3CA* mutations in CMs, we used FACS to sort CD31+ cells (endothelial cell) and CD31– cells from four fresh samples derived from cerebral and spinal cord CMs ([Fig. 3A](#) and [Supplementary Fig. 3](#)). The ddPCR analysis showed that the CD31+ cells derived from the four samples all had a higher fractional abundance of mutations in *MAP3K3* (I441M) or *PIK3CA* (H1047R), which indicated that the somatic mutations mainly occurred in endothelial cells ([Fig. 3A](#) and [Supplementary Fig. 4](#)).

### MAP3K3 mutation showed an impact on angiogenesis

Cells transfected with *MAP3K3* (I441M), as compared with the control, showed significant activation of phosphorylated ERK5, JNK and p38 ([Fig. 3B](#)). However, the extracellular signal-regulated kinase1/2 (ERK1/2) activation was not found. Upregulated *KLF2* and *KLF4* were reported in previous studies,<sup>20</sup> but no significant difference was observed in our results ([Supplementary Fig. 5A and C–H](#)). Overexpression of *MAP3K3* (I441M) increased cell proliferation and cell migration ( $P < 0.001$ ) with VEGFA (20 ng/ml) stimulation compared with the control group ([Fig. 3C](#)). On cell tube formation, overexpression of the mutation in HUVECs led to disruption and disordering of spontaneous vascular tube formation ( $P = 0.001$ ), with significant reductions of total vascular tube length and total mesh area ([Fig. 3D](#)). On cell senescence, overexpression of the *MAP3K3* mutation evidently modified endothelial cell morphology and increased the amount of  $\beta$ -galactosidase (a recognized senescence marker) positive cells ([Supplementary Fig. 6 and E](#)). The activating functions of mutations in *PIK3CA* were also performed and overexpression of mutations in *PIK3CA* also promoted cell proliferation, migration, senescence and disrupted tube formation compared with wild-type ([Supplementary Figs 5B and 6](#)).

### Validation of the impact of MAP3K3 mutation on angiogenesis in a zebrafish model

To investigate the loss-of-function of *Map3k3* in a zebrafish model, morpholino oligonucleotides (MOs) were designed to knockdown wild-type *MAP3K3* in zebrafish embryos. We observed that all of the embryos died within 48 h post-fertilization (hpf) (MO concentration range: 0.05–5 ng), which indicated an indispensable role of *Map3k3* in zebrafish embryonic development. Subsequently, to investigate the function of the *MAP3K3* (I441M) mutation, we

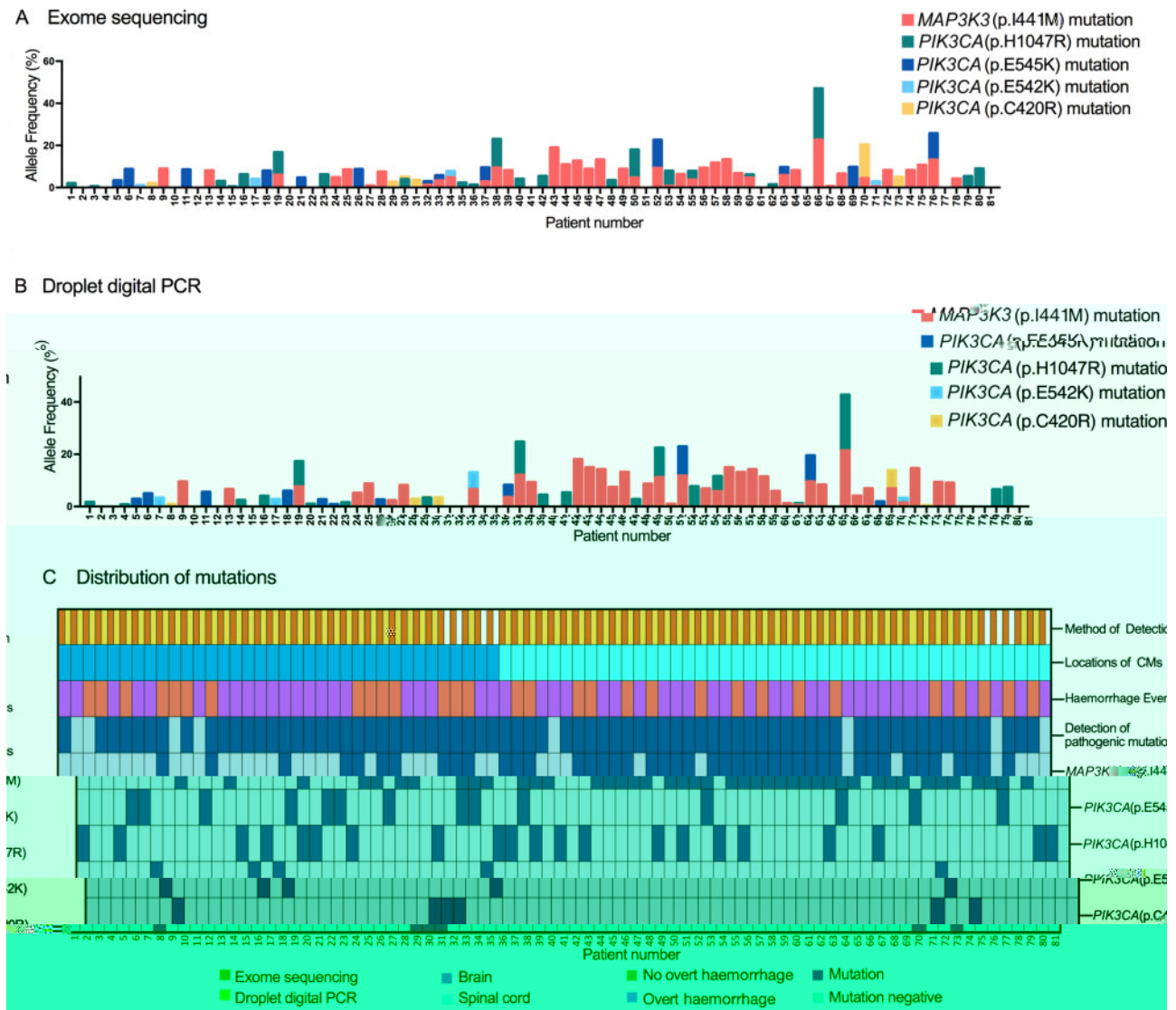


**Figure 1** Detection of pathogenic mutations in samples obtained from patients with CMs. (A) The detection and allele frequency of the pathogenic mutations on WES. Of the 81 sporadic patients detected, 73 (90.1%) were identified as having pathogenic somatic mutations in MAP3K3 and/or PIK3CA. (B) Confirmation and allele frequency of MAP3K3 and PIK3CA mutations by ddPCR. The ddPCR findings were consistent with the WES results ( $r = 0.882$ ,  $P < 0.001$ ). (C) Detailed information regarding the tissue samples. The patient number is in order of the CM locations.

injected wild-type and MAP3K3 (I441M) mRNAs into zebrafish embryos. As expected, in the control group injected with PBS, the upper blood vessels were neatly distributed and the density was uniform. However, in the experimental group injected with wild-type or MAP3K3 (I441M) mRNAs, part of the upper blood vessels were absent and the blood vessel density was uneven (Fig. 3E). Overexpression of the MAP3K3 (I441M) mutation caused more severe phenotypes than wild-type mRNA in zebrafish at the same concentration ( $P < 0.05$ ) (Fig. 3F). The observations of endothelial cell models and zebrafish embryos suggested that the MAP3K3 (I441M) mutation was an activating mutation.

### Single cell RNA sequencing revealed distinct transcriptional signatures between MAP3K3 and PIK3CA mutations

In single cell RNA sequencing, 74 326 single cells from nine samples (six CMs samples and three control samples) were profiled and 65 297 cells passed stringent quality control filters for further

processing. The six samples of CMs included two CMs with MAP3K3 mutations (one with cerebral CMs, one with associated cutaneous CMs), three cerebral CMs with PIK3CA mutations, and one with cerebral CMs with double mutations. The cutaneous lesion was from Patient 75 with spinal CMs at the same spinal metameric segment (Table 3).

The entire population was classified into three cell types, including endothelial cells, mural cells and other cells based on their respective molecular features: VWF, CLDN5, CDH5 (endothelial cells) and PDGFRB, ACTA2, PDLIM3 (mural cells) (Fig. 4A and B).<sup>21–23</sup> ‘Other cells’ were identified as mast cells, astrocytes, plasmacytoid dendritic cells (pDCs), B cells, natural killer (NK) cells, dendritic (DC) cells, oligodendrocytes, microglia, macrophages/monocytes, epithelial cells and T cells by interrogating the expression patterns of known marker genes (Fig. 4A and Supplementary Fig. 7).<sup>24–27</sup> Interestingly, all three CM samples with PIK3CA mutations had minimal counts of endothelial cells and ratio to the total number of sample cells (Fig. 4C). Most differentially expressed genes (DEGs) in endothelial cells were consistent in different

**Table 1 Clinical characteristics and genotype of 73 sporadic CMs patients with somatic mutations**

Variable	Overall	Genotype			P-value
		MAP3K3 mutation	PIK3CA mutation	Co-occurred mutations	
Patients, n (%)	73	28 (38.4)	30 (41.1)	15 (20.5)	
Female, n (%)	31 (42.5)	13 (46.4)	14 (46.7)	4 (26.7)	0.366
Mean age at onset $\pm$ SD (range), years	36.3 $\pm$ 14.4 (8–75)	33.6 $\pm$ 14.6 (8–64)	38.1 $\pm$ 13.1 (10–58)	37.9 $\pm$ 16.8 (9–75)	0.423
Duration of symptoms $\pm$ SE, months	22.4 $\pm$ 4.4	26.3 $\pm$ 8.0	14.7 $\pm$ 4.9	30.5 $\pm$ 12.1	0.303
Locations of presenting or largest CMs (%)					

comparison groups, which indicated similar general genetic alterations in the sporadic CMs with either MAP3K3 or PIK3CA or both mutations (Fig. 4D). The number of DEGs in different comparisons is shown in Supplementary Fig. 8A. Furthermore, Gene Ontology (GO) analysis of DEGs in three mutation groups versus the control group showed consistency of important pathways such as angiogenesis, blood vessel morphogenesis and blood vessel development (Supplementary Fig. 8B). GO analysis of DEGs between subgroups of MAP3K3 and PIK3CA mutations showed the apoptotic signalling pathway was high ranking (Fig. 4E), which was confirmed by terminal deoxynucleotidyl transferase dUTP nick end labelling (TUNEL) immunostaining of eight samples of sporadic CMs with somatic mutations and three control samples of normal brain tissue. Strong positive staining of apoptosis was observed in endothelial cells of CM samples with MAP3K3 mutations ( $n = 4$ ), and negative staining was observed in the other two genetic subgroups (three patients with PIK3CA mutations, one patient with double mutations) and control samples ( $n = 3$ ), shown in the representative graphs (Fig. 4F). In DEGs between three genetic subgroups and the control group, GDF15 and SERPINA5 were notably overexpressed in samples with PIK3CA mutations (Fig. 4C), which was consistent with the results following grouping by genotypes

(Fig. 4H). These results were also verified by immunofluorescence staining (Fig. 4I).

## Discussion

To our knowledge, this is the first study that has demonstrated high prevalence of pathological somatic activating MAP3K3 and PIK3CA mutations in the majority of sporadic CMs in CNS and illustrated the correlations of genotypes with phenotypes. The somatic mutations of MAP3K3 and PIK3CA mainly occurred in endothelial cells. The MAP3K3 mutations activated the phosphorylated ERK5, JNK and p38 pathway in endothelial cells and caused vascular malformations in zebrafish. Distinct transcriptional signatures between different genetic subgroups were identified. Significant apoptosis in MAP3K3 mutation carriers and overexpression of GDF15 and SERPINA5 in PIK3CA mutation carriers contributed to their phenotype.

We did not find any somatic non-synonymous mutations of the three CCM genes (KRIT1, CCM2, PDCD10) in the 81 patients with sporadic CMs. According to previous studies, several somatic mutations in the three CCM genes were found in sporadic CMs,

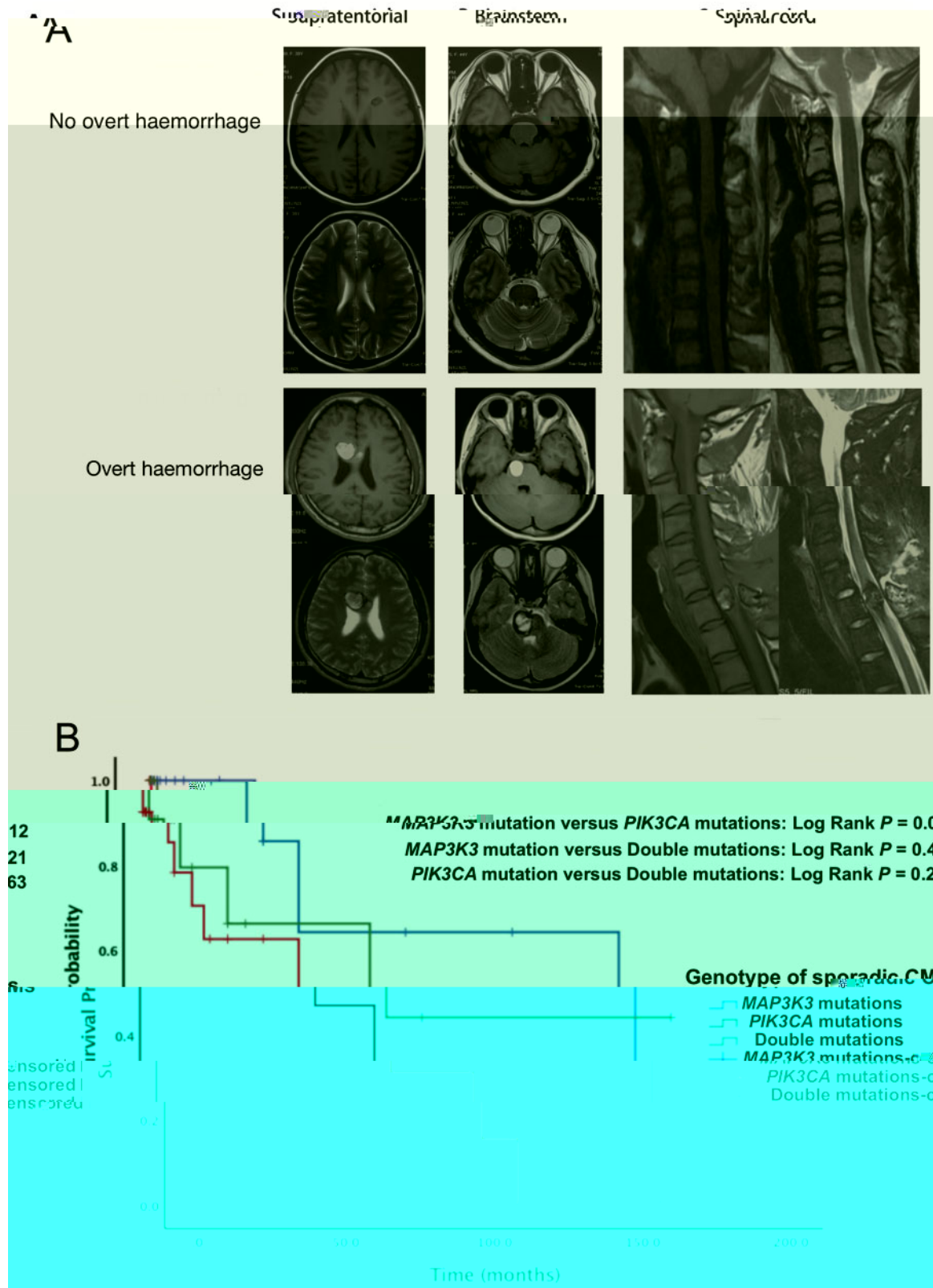


**Figure 2** Haemorrhage events of CMs in brain and spinal cord. (A) MRI obtained in patients with CMs in lobes, brainstem and spinal cord with/without overt haemorrhage. (B) Kaplan-Meier analysis illustrating subsequent haemorrhage risks of sporadic CMs in different genotypes. The log-rank test indicated that haemorrhagic events during the follow-up period were more frequent in patients with PIK3CA mutations than with MAP3K3 mutations ( $P = 0.012$ ) and the haemorrhagic risk during the follow-up period of double mutations was in-between; however, the P-value for difference between the three genotypes did not achieve statistical significance, though a trend was observed ( $P = 0.051$ ).

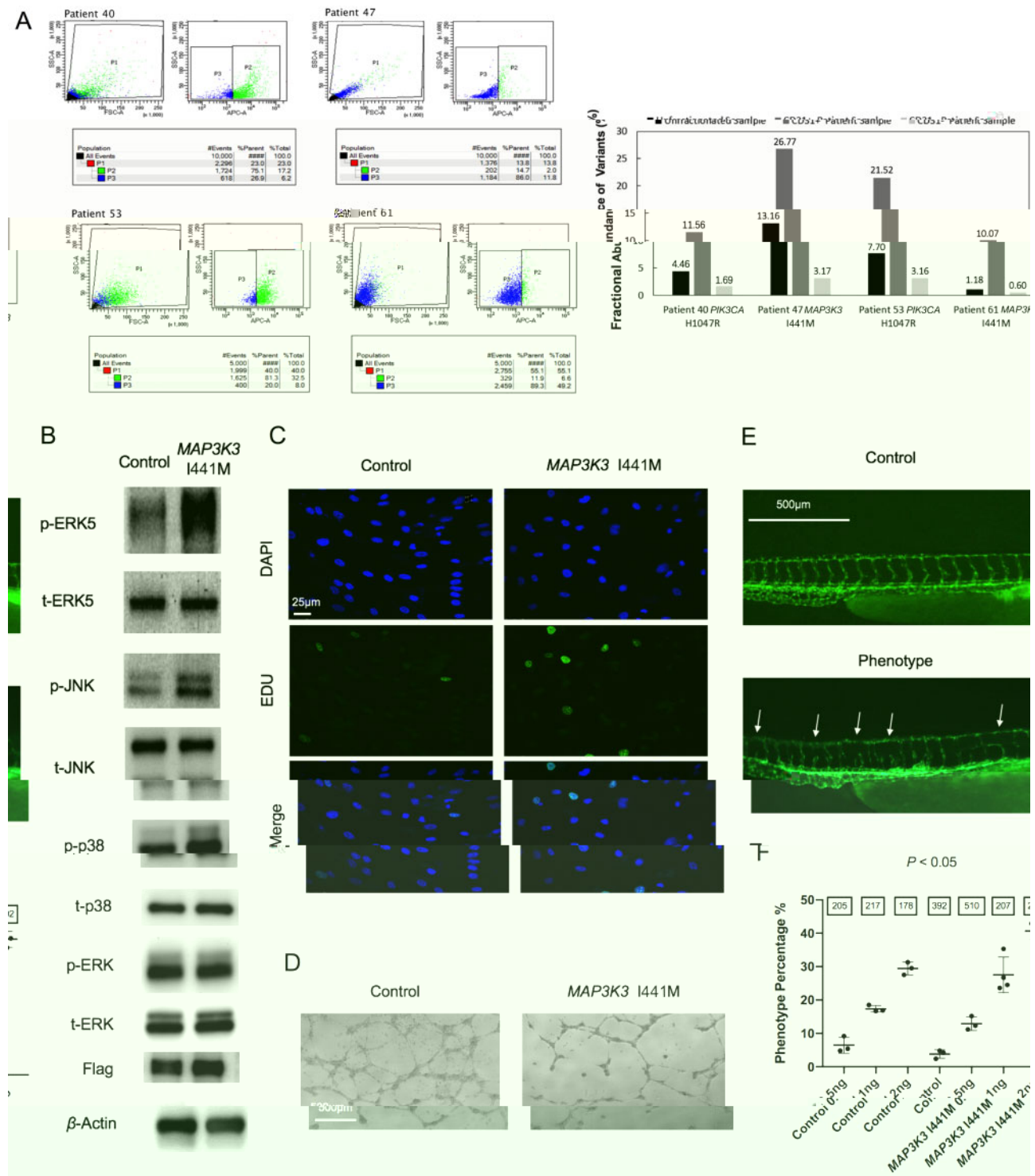


**Figure 3** Cell locations of *MAP3K3* and *PIK3CA* mutations and phenotypes of endothelial cells and zebrafish expressing activating *Map3k3*. (A) The FACS plots of flow sorting of four samples of sporadic CMs and the fractional abundance of *MAP3K3* and *PIK3CA* variants in CD31+ and CD31- cells derived from four fresh tissue samples and in the whole tissue sample before sorting. (B) Downstream effectors of *MAP3K3*. Plasmids encoding *MAP3K3* (I441M) and wild-type *MAP3K3* (Control) with FLAG-tag were transfected into HUVECs. Significantly increased phosphorylation of extracellular signal regulated kinase 5 (ERK5) was observed with *MAP3K3* (I441M). Increased phosphorylation of p38 and Jun N-terminal kinase (JNK) were also seen with *MAP3K3* (I441M). While no change in phosphorylation of ERK1/2 was observed with the *MAP3K3* (I441M). (C) Increased cell proliferation in mutant *MAP3K3* (I441M) compared with wild-type via 5-ethynyl-2'-deoxyuridine (EDU) staining 48 h after transfection and VEGFA (20 ng/ml) treatment for 12 h. Green indicates EDU and blue indicates nucleus [4',6-diamidino-2-phenylindole dihydrochloride (DAPI)]. (D) Visible disruption of endothelial vascular tube formation in cells transfected with mutant *MAP3K3* (I441M) compared with wild-type (Control). (E) The vascular deficits of zebrafish injected with wild-type or mutant *MAP3K3* (I441M) mRNA and control (PBS) at 48 h post-fertilization (hpf). The cardiovascular system was marked with EGFP (kdr1). Errors show the locations of absent blood vessels and uneven blood vessel density. (F) The quantification of zebrafish with vascular phenotypes (one-way ANOVA test). The number in the box above the column represents the number of patients in each group.

while the literature quantity was much fewer and the sample size was smaller than those of the familial CMs.<sup>12-14</sup> Regarding the 300× depth of WES in our study, the possibility of finding somatic mutations in these genes in our study was potentially higher than that in some previous studies. We observed the discrepancy of the somatic mutations in the three CCM genes between our study and previous studies on sporadic CMs, which might be due to genetic background from different populations.

Recently, in a cohort of 31 sporadic patients with CMs, five



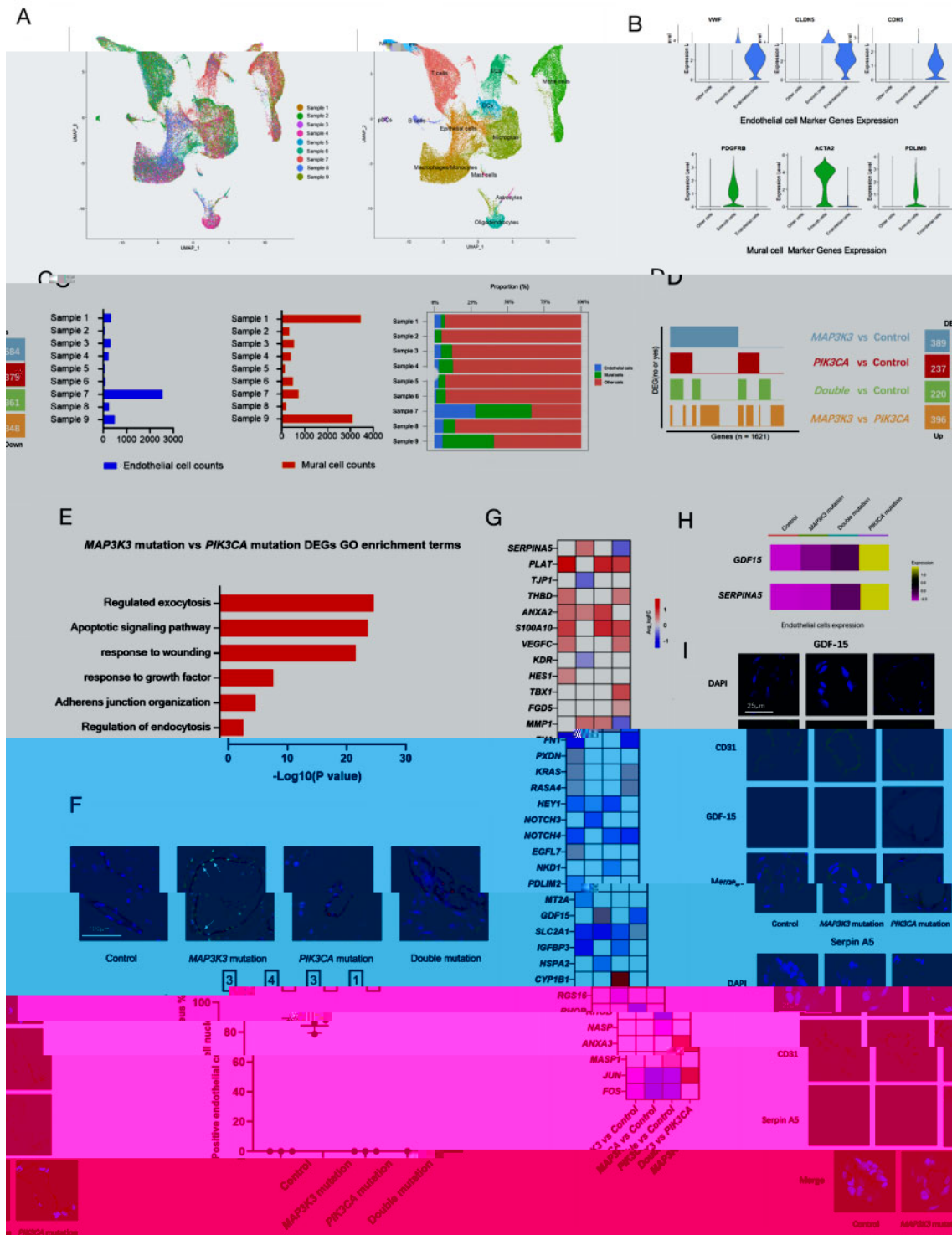


**Figure 4** Single cell RNA sequence revealed distinct transcriptional signatures between MAP3K3 and PIK3CA mutations. (A) UMAP (uniform manifold approximation and projection) clustering of 65 297 cells isolated from nine samples (six CMs samples and three control samples). Cells were marked by tissue sources (left) or cell types (right). (B) Violin plots of endothelial cell and mural cell marker genes expressions identified by differential expression analysis. (C) Bar graphs depicting the counts of endothelial cells and mural cells from nine samples. Right: The proportion of endothelial cells, mural cells and other cells. (D) Binary plots indicating with bars whether a gene (column) is a differentially expressed gene (DEG) in a given comparison group (rows) or not (n = 1621 DEGs). Right: DEG counts for each comparison group. (E) Selected top categories from GO enrichment analysis of DEGs to compare the differences of biological functions between MAP3K3 and PIK3CA mutation groups. (F) TUNEL immunostaining of CM tissues with MAP3K3 mutations (Patient 43), PIK3CA mutations (Patient 11), double mutations of MAP3K3 and PIK3CA (Patient 66), and one control tissue of temporal lobe. Overlay of DAPI (blue), CD31 (red) and apoptotic nucleus (green) are shown. The quantification of apoptotic endothelial cells from MAP3K3 mutation groups were much higher than other groups (P < 0.001). The number in the box above the column represents the number of patients in each group. MAP3K3 mutation groups included Patients 13, 43, 45 and 57. PIK3CA mutation groups included Patients 11, 22 and 40. The double mutation group included Patient 66. (G) Heat maps of the expression of related DEGs from different subgroups compared with the control group. (H) Heat maps of GDF15 and SERPINA5 expressions in three genetic subgroups and the control group. (I) Immunostaining of CM tissues with MAP3K3 (Patient 5), PIK3CA (Patient 45) mutations and control tissue for GDF-15 and Serpin A5. MAP3K3 mutation groups included Patients 43, 46 and 68. PIK3CA mutation groups included Patients 5, 11 and 52. Consistent with the results of single cell RNA sequencing, both were positive in patients of PIK3CA mutation and negative in other samples. Single-channel images of DAPI (blue), CD31 (red), GDF-15 (green) or Serpin A5 (green) and overlay of them are all shown.

CNS. The mutations spectrum may correlate with the phenotype of sporadic CMs and *PIK3CA* mutations may confer a higher risk for overt haemorrhage. The functional studies and single cell transcriptomic analysis provide a blueprint for interrogating the cellular and molecular basis of sporadic CMs.

## Acknowledgements

We thank all the patients and their families for participating in our study, and for offering all information, data, and updates on the disease in these patients.

## Funding

This work was supported by National Key R&D Program of China (2017YFC0909400), National Natural Science Foundation of China with grants (81770424, 81970430, 81971104, 81971113 and 81671202), Chinese Academy of Medical Sciences with Innovation Fund for Medical Sciences Health and Longevity Pilot Project (CIFMS2017-I2M-1-008 and 2019-RC-HL-002), Beijing Municipal Science and Technology Commission (Z201100005520024), Beijing Municipal Administration of Hospitals (DFL2018080 and QML20190802) and Beijing Municipal Education Commission (CIT&TCD201904095).

## Competing interests

The authors report no competing interests.

## Supplementar material

[Supplementary material](#) is available at *Brain* online.

## References

1. Vernooij MW, Ikram MA, Tanghe HL, et al. Incidental findings on brain MRI in the general population. *N Engl J Med.* 2007; 357(18):1821–1828.
2. Otten P, Pizzolato GP, Rilliet B, Berney J. 131 cases of cavernous angioma (cavernomas) of the CNS, discovered by retrospective analysis of 24,535 autopsies. *Neurochirurgie.* 1989;35(2):82–131.
3. Morris Z, Whiteley WN, Longstreth WT Jr, et al. Incidental find-

29. Janku F, Lee JJ, Tsimberidou AM, et al. PIK3CA mutations frequently coexist with RAS and BRAF mutations in patients with advanced cancers. *PLoS One*. 2011;6(7):e22769.
30. Ten Broek RW, Eijkelenboom A, van der Vleuten CJM, et al. Comprehensive molecular and clinicopathological analysis of vascular malformations: A study of 319 cases. *Genes Chromosomes Cancer*. 2019;58(8):541–550.
31. Pagenstecher A, Stahl S, Sure U, Felbor U. A two-hit mechanism causes cerebral cavernous malformations: Complete inactivation of CCM1, CCM2 or CCM3 in affected endothelial cells. *Hum Mol Genet*. 2009;18(5):911–918.
32. McDonald DA, Shenkar R, Shi C, et al. A novel mouse model of cerebral cavernous malformations based on the two-hit mutation hypothesis recapitulates the human disease. *Hum Mol Genet*. 2011;20(2):211–222.
33. Spiegler S, Rath M, Much CD, Sendtner BS, Felbor U. Precise CCM1 gene correction and inactivation in patient-derived endothelial cells: Modeling Knudson's two-hit hypothesis in vitro. *Mol Genet Genomic Med*. 2019;7(7):e00755.
34. Goyal A, Rinaldo L, Alkhataybeh R, et al. Clinical presentation, natural history and outcomes of intramedullary spinal cord cavernous malformations. *J Neurol Neurosurg Psychiatry*. 2019; 90(6):695–703.
35. Horne MA, Flemming KD, Su IC, et al.; Cerebral Cavernous Malformations Individual Patient Data Meta-analysis Collaborators. Clinical course of untreated cerebral cavernous malformations: A meta-analysis of individual patient data. *Lancet Neurol*. 2016;15(2):166–173.
36. Al-Shahi Salman R, Hall JM, Horne MA, et al. Untreated clinical course of cerebral cavernous malformations: A prospective, population-based cohort study. *Lancet Neurol*. 2012;11(3):217–224.